UC Santa Cruz

UC Santa Cruz Previously Published Works

Title

Improved efficient physics-based computational modeling of regional wave-driven coastal flooding for reef-lined coastlines

Permalink

https://escholarship.org/uc/item/14h4w43t

Authors

Gaido-Lasserre, Camila

Nederhoff, Kees

Storlazzi, Curt D

et al.

Publication Date

2024-06-01

DOI

10.1016/j.ocemod.2024.102358

Copyright Information

This work is made available under the terms of a Creative Commons Attribution-NonCommercial-NoDerivatives License, available at https://creativecommons.org/licenses/by-nc-nd/4.0/

Peer reviewed

eScholarship.org Powered by the California Digital Library
University of California

Ocean Modelling 189 (2024) 102358

Contents lists available at ScienceDirect

Ocean Modelling

journal homepage: www.elsevier.com/locate/ocemod

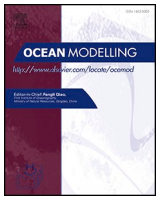

Improved efficient physics-based computational modeling of regional wave-driven coastal flooding for reef-lined coastlines

Camila Gaido-Lasserre [a,*], Kees Nederhoff [b], Curt D. Storlazzi [c], Borja G. Reguero [a], Michael W. Beck [a]

[a] Institute of Marine Sciences, University of California, Santa Cruz, CA 95060, USA
[b] Deltares USA, Silver Spring, MD 20910, USA
[c] U.S. Geological Survey, Pacific Coastal and Marine Science Center, Santa Cruz, CA 95060, USA

ARTICLE INFO

Keywords:
Regional flood risk
Wave-driven flooding
SFINCS
XBeach
Flood extent
Flood depth

ABSTRACT

Coastal flooding affects low-lying communities worldwide and is expected to increase with climate change, especially along reef-lined coasts, where wave-driven flooding is particularly prevalent. However, current regional modeling approaches are either insufficient or too computationally expensive to accurately assess risks in these complex environments. This study introduces and validates an improved computationally efficient and physics-based approach to compute dynamic wave-driven regional flooding on reef-lined coasts. We coupled a simplified-physics flood model (SFINCS) with a one-dimensional wave transformation model (XBeach-1D). To assess the performance of the proposed approach, we compared its results with results from a fully resolving two-dimensional wave transformation model (XBeach-2D). We applied this approach for a range of storms and sea-level rise scenarios for two contrasting reef-lined coastal geomorphologies: one low relief area and one high relief area. Our findings reveal that SFINCS coupled with XBeach-1D generates flood extents comparable to those produced by XBeach-2D, with a hit rate of 92%. However, this method tends to underpredict the flood extent of weaker, high-frequency storms and overpredict stronger, low-frequency storms. Across scenarios, our approach overpredicted the mean flood water depth, with a positive bias of 7 cm and root mean square difference of 15 cm. Offering approximately 100 times greater computational efficiency than its two-dimensional XBeach counterpart, this flood modeling technique is recommended for wave-driven flood modeling in scenarios with high computational demands, such as modeling numerous scenarios or undertaking detailed regional-scale modeling.

1. Introduction

Coastal flooding affects low-lying communities around the world and is expected to increase due to climate change effects on sea-level rise (SLR), wave action, and ecosystem degradation (Ferrario et al., 2014; Lashley et al., 2018; Reguero et al., 2021; Sheppard et al., 2005; Storlazzi et al., 2015, 2018; Taherkhani et al., 2020). Accurate regional (e.g., spatial scales on the order of 10s – 1000s km) flood risk assessments are essential to inform communities of risk, develop flood risk management strategies, and prioritize management actions amongst locations. Therefore, regional flood modeling must be improved, particularly in complex wave-driven flooding environments such as reef-lined coasts.

Wave-driven processes can have a significant contribution to inland flooding on reef-lined coasts. Particularly, coral reef-lined coasts can experience severe flooding due to the combination of tide, storm surge, wave setup, wave runup, and sometimes wave resonance (Cheriton et al., 2016; Quataert et al., 2015; Torres-Freyermuth et al., 2012). These complex environments are characterized by an abrupt fore-reef slope, shallow reef crest, and relatively horizontal reef flat; such features dissipate incoming offshore wave energy due to wave breaking and bottom friction (Hardy and Young, 1996; Péquignet et al., 2011), mainly affecting high-frequency sea-swell waves (>0.04 Hz), which energy has been found to reduce toward the coast (Nwogu and Demirbilek, 2010). Part of the high-frequency wave energy is transferred to the low-frequency energy band (<0.04 Hz), leading to a dominance of low-frequency waves on the reef flat. The dominance of these waves on the reef flat drives coastal flooding in these environments due to their relevant contribution to overwash and runup (Cheriton et al., 2016; Nwogu and Demirbilek, 2010).

Even though coral reefs are the first line of protection against

* Corresponding author.
E-mail address: cgaido@ucsc.edu (C. Gaido-Lasserre).

https://doi.org/10.1016/j.ocemod.2024.102358
Received 21 October 2023; Received in revised form 15 February 2024; Accepted 11 March 2024
Available online 12 March 2024
1463-5003/Published by Elsevier Ltd. This is an open access article under the CC BY-NC-ND license (http://creativecommons.org/licenses/by-nc-nd/4.0/).

flooding, they can also enhance flooding during storm conditions due to their impact on wave dynamics (Péquignet et al., 2009; Roeber and Bricker, 2015; Shimozono et al., 2015). Wave breaking on the fore reef generates high radiation stress gradients, which are balanced by an increase in mean water level on the reef flat (i.e., wave setup). The latter allows the propagation of larger waves on the reef flat, which can enhance runup and, consequently, flooding. Thus, to properly model runup wave-driven flooding, both the changes in water level due to wave setup and the oscillations around this water level (i.e., swash) must be considered.

Coastal wave-driven flooding at a local scale (~10 km) can be accurately modeled with physics-based wave-resolving models such as two-dimensional XBeach (XBeach-2D; Roelvink et al., 2009, 2018), SWASH (Zijlema et al., 2011) and FUNWAVE-TVD (Shi et al., 2012). The first two models are based on the nonlinear shallow water equations and the latter on nonlinear Boussinesq equations. These models are adept at resolving complex wave-hydrodynamics and computing the corresponding wave-driven flooding. Moreover, they include ecosystem modeling through friction and vegetation modeling, which is relevant in coral reef-lined coasts (Reguero et al., 2021; Storlazzi et al., 2019). However, the high computational demand of these models limits their applicability for larger, regional-scale studies. These studies, such as evaluating flood risk under specific storm conditions for an entire Hawaiian island, typically utilize circulation models like ADCIRC (Luettich et al., 1992) and Delft3D (Kernkamp et al., 2011) coupled with a stationary wave solver (e.g., SWAN; Booij et al., 1999). These models have lower computational costs than two-dimensional physics-based wave-resolving models. However, they focus on tide and surge modeling and do not account for unsteady wave-driven processes such as swash and runup.

Between these two physics-based modeling approaches, there are several methods ranging from metamodels or surrogate models to wave-resolving models coupled with flood models. Metamodels are simplified approximations of complex models that emulate input/output behavior. These models are data based and rely on the analysis between a limited amount of simulations to predict an outcome (e.g., Camus et al. 2014, Gouldby et al. 2014, Rueda et al. 2019a, van Vloten et al. 2022). Metamodels for flooding can include statistical-based models (Camus et al., 2014; Rohmer and Idier, 2012), Radial Basis Functions (Rueda et al., 2019b), and machine learning methods (Zahura et al., 2020). These models are trained to be a valuable and fast tool and have the potential to be successfully used for coastal flooding proxies (Rohmer and Idier, 2012), early warning systems (Betancourt et al., 2020; Idier et al., 2021), and real-time inundation forecasting and management (Zahura et al., 2020). However, even though these models can be trained with physics-based data and/or relations, the resulting flooding will always be an approximate result. These methods lack the fundamental inclusion of physical principles and laws that govern the behavior of natural phenomena, which might influence their consistency across different scenarios for which they are not trained yet and thus the predictive power for unseen (extreme) cases.

An alternative approach involves the integration of one-dimensional (1D) wave-resolving models with two-dimensional (2D) inland flood models. This strategy varies in complexity, ranging from basic techniques like the bathtub or interpolation methods to more advanced 2D reduced-physics models. Such hybrid modeling has been employed in various studies. For example, Barnard et al. (2019) predicted flood depths with 1D XBeach transects, which were interpolated onto regular grids and subtracted from high-resolution digital modeling to calculate flood maps. Toimil et al. (2023) computed total water levels from XBeach and derived statistically robust extreme total water levels to define tidal profiles similar to the Storm Gloria peak, which were used as boundary conditions for the hydraulic model RFSM-EDA (Jamieson et al., 2012). Armaroli et al. (2019) used discharge time series obtained after the dune crest from XBeach transect outputs to force Lisflood-FP (Bates et al., 2005). However, it is notable that these studies primarily focused on beach and dune systems, omitting the modeling of ecosystems and their impact on wave dynamics and flooding. Additionally, several of these studies employed a statistical imposition of runup heights, thereby overlooking the dynamic aspects of flooding. Alternatively, although some coupled models do incorporate water level time series, they often neglect the inclusion of low-frequency wave time series. This aspect is particularly crucial in areas where features like coral reef coastlines significantly influence flood wave dynamics.

Our study aims to introduce and validate a physics-based computationally efficient approach to dynamically assess wave-driven regional flooding on reef-lined coastlines with acceptable accuracy. We propose a method that couples at a specific depth (i.e., coupling line) the new Super-Fast INundation of CoastS model (SFINCS; Leijnse et al., 2021) with one-dimensional XBeach models (XBeach-1D), including both static water level and (unsteady) wave time series as boundary conditions on coral reef environments. SFINCS calculates compound flooding by applying simplified mass and momentum equations (Local Inertial Equations; LIE) and, with the inclusion of advection, it can effectively model dynamic wave-driven flooding (Simplified Shallow Water Equations; SSWE). In this framework, XBeach is used in 1D 'surfbeat' mode in which the spatio-temporal wave energy changes are computed on the incident wave group period scale. The wave force resulting from wave energy variation in time is used to resolve low-frequency waves and wave setup (Roelvink et al., 2009). The wave data generated by XBeach are crucial for SFINCS, which by itself does not produce infragravity waves and setup.

SFINCS-LIE has previously been used to determine the compound flooding hazards of tropical storm systems (Eilander et al., 2023; Sebastian et al., 2021). However, these studies did not account for the impact of swash and runup on flooding and, consequently, did not dynamically model wave-driven flooding. Leijnse et al. (2021) demonstrated that SFINCS-SSWE is able to simulate wave runup and wave-driven flooding when advection is included. In this study, we use SFINCS-SSWE to account for advective processes. To evaluate the accuracy and computational efficiency of the proposed flooding approach, we compare it to XBeach-2D results for different SLR and storm scenarios. Additionally, to assess its performance in different reef geomorphologies, this study compares both coastal flooding approaches in two endmembers of the reef-lined coastlines: a low relief area (Miami Beach, FL, USA) and a high relief area (Kailua-Waimanalo area on O'ahu, HI, USA).

2. Methods

2.1. Study sites and modeled scenarios

To assess the accuracy of the SFINCS approach (SFINCS-SSWE coupled with XBeach-1D), we compared the results of the proposed flooding approach to XBeach-2D results for different storm and SLR scenarios at two study sites (Fig. 1). The sites have different coastal geomorphologies and are two endmembers of coral reef-lined coastlines: a low relief area and a high relief area. Miami Beach, Florida, USA (25.79° N, 80.13° W), is a low relief area with a broader shelf, relatively uniform alongshore coastline, and a coastal system characterized by offshore reefs, barrier islands, and a low-lying coastal zone. On the other end of the spectrum, Kailua-Waimanalo, O'ahu, Hawai'i, USA (21.44° N, 158.00° W), represents a high relief area with a steeper insular shelf, distinct fringing reefs, a curvilinear coastline with bays and headlands, and relatively higher-elevation coastal zone.

The selected storms are based on prior analyses (Reguero et al., 2021; Storlazzi et al., 2019), where wave climate and water levels were calculated as univariate probability. In these studies, hourly offshore wave data from 1948 to 2008 were obtained from the Global Ocean Wave (GOW) database (Reguero et al., 2012). The wave data were synthesized into 500 sea state combinations (wave heights, wave periods, and wave directions) that best represented the 61 years of

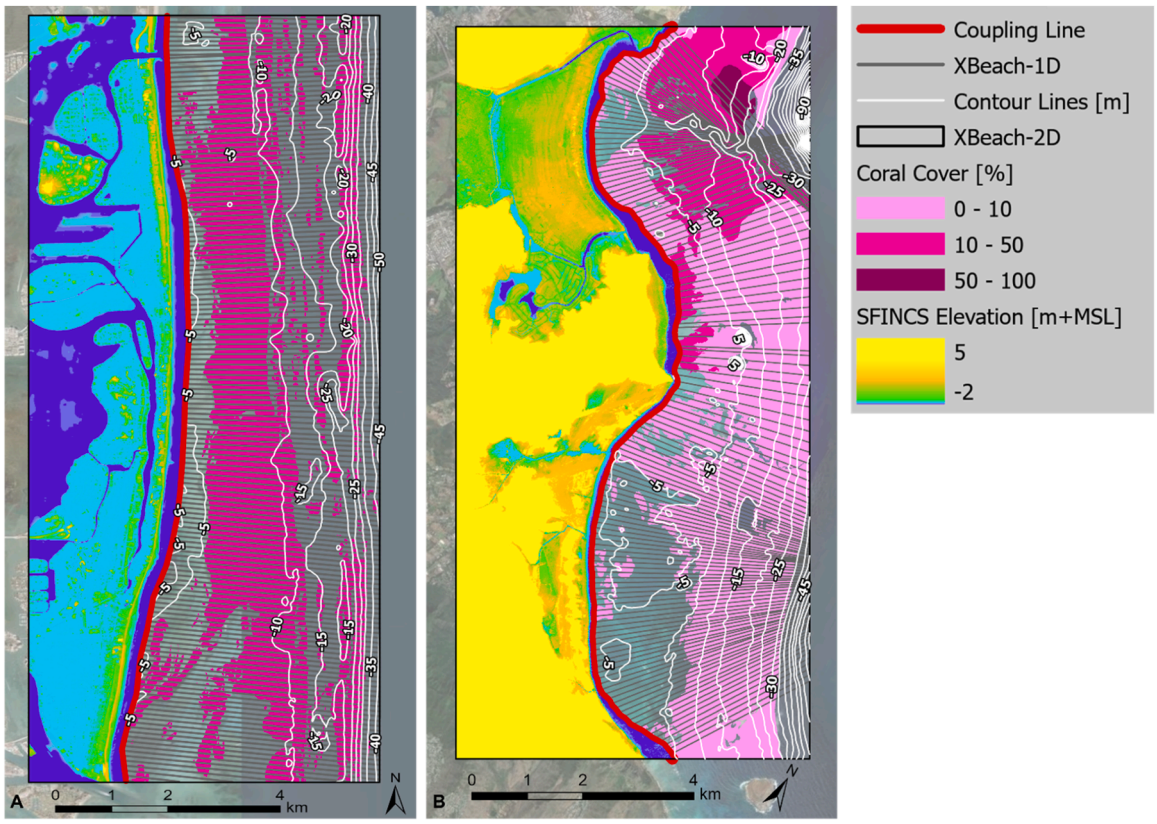

Fig. 1. Study sites and hydrodynamic models used for the comparison of the proposed SFINCS flood modeling approach (SFINCS-SSWE coupled with XBeach-1D) to XBeach-2D in Miami Beach, Florida, USA (A) and Kailua-Waimanalo, O'ahu, Hawai'i, USA (B). The black polygon represents the XBeach-2D model area. The gray lines are XBeach-1D transects coupled with SFINCS at the coupling line (red). The percentage of coral cover is represented in a pink gradient, the 5-m isobaths are displayed as white lines, and the SFINCS model bed elevation can be seen in a range of colors from 2 m depth to 5 m elevation. Miami Beach is characterized by relatively low coastal relief, and Kailua-Waimanalo by relatively high coastal relief.

deep-water conditions. The latter was achieved using a maximum dissimilarity algorithm based on Camus et al. (2011). The selected 500 sea states were propagated to the fore reef using the physics-based third-generation spectral wave model Simulating Waves Nearshore (SWAN; Booij et al., 1999), which has been proven to simulate short wave propagation around coral reef-lined islands accurately (Hoeke et al., 2011; Lowe et al., 2009; Storlazzi et al., 2015). Finally, the propagated wave conditions were extracted every 100 m along the coastline at ~30 m water depth and reconstructed into 61 year hourly time series using radial basis functions (Camus et al., 2011). Each of these nearshore time series was fit to a generalized Pareto distribution to calculate the 10-, 50-, 100-, and 500-yr storm return periods wave height and wave period (average values are shown in Table 1). For each return period, the corresponding extreme water level was extracted from the nearest National Oceanic and Atmospheric Administration tidal station (NOAA, 2020), which is based on a Generalized Extreme Value probability distribution function. The daily and 1-yr return period storms were linearly extrapolated from the 10-yr return period storm. Each scenario was run at three different sea levels to assess the impact of SLR: 0.0, +0.5, and +1.0 m. This range of conditions allows for a reliable accuracy estimate of the SFINCS flooding approach across different events (i.e., daily events and rare storms). The hydrodynamic forcing for each return period was then propagated with the numerical model XBeach.

2.2. Model setup

XBeach is a numerical model that simulates nearshore hydrodynamics by solving the depth-averaged nonlinear shallow-water equations. XBeach was originally derived for sandy beaches but has been successfully advanced and applied to predict coral reef hydrodynamics accurately (Quataert et al., 2015; van Dongeren et al., 2013). XBeach has

Table 1
Design return-period (RP) storms used for both study sites and flooding methodologies to allow direct comparison between the models' results. SWL is the still water level relative to the mean sea level, Hs is the spatially averaged significant wave height, and Tp is the spatially averaged peak wave period. The number in brackets indicates the corresponding standard deviation for each spatially averaged value.

	Miami Beach, FL.			Kailua-Waimanalo, HI.		
RP	SWL (m)	Hs (m)	Tp (s)	SWL (m)	Hs (m)	Tp (s)
Daily	0.28 [0.00]	2.25 [0.00]	11.25 [0.00]	0.68 [0.00]	1.33 [0.00]	12.66 [0.00]
1 year	0.77 [0.00]	2.97 [0.00]	12.72 [0.00]	0.72 [0.00]	3.14 [0.00]	15.37 [0.00]
10 years	1.11 [0.00]	3.65 [0.21]	13.68 [0.54]	0.74 [0.00]	3.98 [0.23]	16.75 [0.27]
50 years	1.33 [0.00]	4.04 [0.28]	14.44 [0.53]	0.76 [0.00]	4.61 [0.34]	17.78 [0.47]
100 years	1.51 [0.00]	4.18 [0.30]	14.78 [0.54]	0.81 [0.00]	4.94 [0.41]	18.36 [0.60]
500 years	2.33 [0.00]	4.48 [0.35]	15.57 [0.59]	1.19 [0.00]	5.85 [0.65]	20.22 [1.08]

three modes including, 'stationary,' 'surfbeat,' and the 'non-hydrostatic' mode. The 'surfbeat' mode solves the short-wave energy variation on a group scale, whereas the 'non-hydrostatic' mode solves each individual short wave. The 'surfbeat' mode was chosen in this study because it saves computational time and has been proven to provide accurate flooding results in reef environments (Quataert et al., 2020). XBeach was run as cross-shore transects or one-dimensional models (XBeach-1D) and as a two-dimensional model (XBeach-2D). The main differences between a 1D and 2D application are 1) lack of spatial variability and 2) lack of directional spreading when running a 1D model. The XBeach-2D model results are used as a flooding benchmark based on their history of accurately simulating coastal hydrodynamics and flooding (Quataert et al., 2015; van Dongeren et al., 2013), and the XBeach-1D models were coupled with the new Deltares flood model SFINCS to provide incoming infragravity waves (0.004 - 0.04 Hz). The details of this coupling can be found in Section 2.3.

SFINCS is a reduced-complexity physics-based model that dynamically calculates compound flooding in coastal systems (Leijnse et al., 2021) with higher computational efficiency than other physics-based approaches. SFINCS works with rectangular grids where each grid cell is defined as an active cell (flooding is calculated), an inactive cell (flooding is not calculated to optimize the run, i.e., on very high elevation areas), or a boundary cell. In this study, grid cells intersecting with the coupling line were defined as boundary cells, grid cells offshore of the coupling line or with an elevation higher than 20 m were inactive, and all the rest of the grid cells were active. To model coastal flooding, SFINCS is forced with time series of both water levels (slowly varying) and infragravity waves (rapidly varying) as boundary condition points. These time series were calculated from water level time series extracted from each XBeach-1D model at the intersection with the coupling line. A boundary condition point was generated every 100 m along the coupling line. Each boundary condition grid cell was forced with a weighted average of the two closest boundary condition points. The advection term in the momentum equations is included, which is necessary to model shock flows such as dam breaks but also incident broken waves (SFINCS-SSWE; Leijnse et al., 2021). However, SFINCS does not include any stationary wave drivers and thus can not generate wave setup and infragravity waves.

The topography and bathymetry data sets (Carignan et al., 2015; Love et al., 2019) used to build the models have a 10 m resolution. Cross-shore transects from Reguero et al. (2021) and Storlazzi et al. (2019) were used as the base for the XBeach-1D models. These transects were created perpendicular to the shore and are spaced every 100 m alongshore, extending from 30 m water depth to 20 m elevation. More details of the transect generation can be found in Reguero et al. (2021) and Storlazzi et al. (2019). The coral cover percentage and extent along these coastlines were taken from benthic habitat maps of the areas (Anderson, 2007; FFWCC-FWRI, 2016) and used to represent the incident sea-swell wave friction coefficient (f_w) and the infragravity wave and current friction coefficient (*Manning n-coefficient*) based on van Dongeren et al. (2013). For the inland area of SFINCS and XBeach-2D models, a Manning coefficient of 0.035 $m^{1/3}/s$ was used.

The XBeach-2D models (grids, bed levels, and friction coefficients) were set up first, and their data were used as input to build XBeach-1D and SFINCS models to decrease possible differences due to interpolation. The XBeach-2D models have an alongshore grid resolution of 10 m and a cross-shore resolution varying from 10 m offshore to 2 m onshore. The XBeach-1D models have the exact cross-shore resolution as XBeach-2D, and the SFINCS models have a constant 2 m cross-shore and 10 m alongshore grid resolution. To accurately compare SFINCS and XBeach-2D results, the SFINCS grids offshore boundary starts where the XBeach-2D grid cross-shore resolution becomes constant (i.e., 2 m), giving a perfect match between models' grid cells across the SFINCS model. An example of each model's main setup file can be found in the Appendix.

Each XBeach-1D transect was forced with a JONSWAP spectrum (Hasselmann et al., 1973) based on the closest wave climate point extracted from the SWAN models (see for the average values in Table 1). Therefore, two consecutive transects do not necessarily have the same forcing and thus vary alongshore. XBeach-2D was forced with the same spatially varying boundary conditions used on XBeach-1D. Waves were imposed shore normal on both models. Furthermore, the default directional spreading of $s = 10$ was applied. The lack of alongshore variation and directional spreading on 1D models leads to an infragravity wave energy overprediction compared to 2D models (Guza and Feddersen, 2012). Even if a directional spreading value is used in XBeach-1D models, it can only be modeled in XBeach-2D. Thus, to compensate for this overprediction, the effects of the directional spreading were included in XBeach-1D models through the model parameter *wbcEvarreduce* = *0.5*, which reduces the short-wave group variance at the boundary by 50% on the XBeach-1D models. This parameter is a first-order estimate to reduce the infragravity wave energy on XBeach-1D models and was used for calibration purposes. To determine the needed reduction factor (*wbcEvarreduce*), a sensitivity analysis was carried out by comparing the resulting significant wave height between XBeach-1D and XBeach-2D models in several nearshore points. The highest skill compared to XBeach-2D results was achieved when using a wave energy reduction of 75% on the low relief area (less extreme wave climate and broader shelf) and 45% on the high relief area (more extreme wave climate and steeper shelf). The 50% was selected as a value with acceptable performance for both areas. For more information on this implementation, one is referred to McCall et al. (2023). The implications of this modeling choice are described in the Discussion.

2.3. Flood modeling approaches

The flooding approaches compared in this study (Fig. 2) used the same input data and boundary conditions and covered the same areas. The XBeach-2D approach used the boundary conditions directly to calculate flood maps (Fig. 2 upper panel – Approach 1). The SFINCS approach used the boundary conditions first in XBeach-1D, and its results provided SFINCS's boundary conditions (Fig. 2 bottom panel – Approach 2). This section discusses the coupling methodology and describes the location where the total water level time series were extracted from XBeach-1D output and used as SFINCS inputs.

The XBeach-1D total water level outputs were used to compute the two time series used as the boundary conditions to force SFINCS: a) the still water level and b) the swash or infragravity wave time series. The still water level time series was built starting from zero and slowly ramping up until reaching the mean water level at the XBeach-1D extraction location. The ramp-up was designed to avoid bathtub-type flooding at the start of the simulation due to the initial water level. The wave time series were computed using the incoming signal from the XBeach-1D outputs, which was calculated by splitting the total water level into incoming and outgoing based on Guza et al. (1984). The swash time series can be constructed in two different ways: 1) directly using the incoming water level time series from XBeach-1D as SFINCS' input, or 2) by using a spectra-based generated time series. Moving forward, we refer to these coupling methods as 'direct' and 'indirect,' respectively. The direct method does not require further data processing after extracting the incoming signal from the total water level as computed by XBeach. However, it computes irregular phase differences between consecutive wave boundary locations due to the direct use of incoming signals from independent XBeach-1D transects. The indirect method requires more data processing because a random signal must be generated based on the spectrum calculated from the XBeach-1D incoming water levels. The generation of a wave time series from a wave spectrum (i.e., the indirect method) is based on the implementation in XBeach (Roelvink et al., 2009; van Dongeren et al., 2003), where each wave component is defined by frequency, amplitude, and phase. The summation of all components gives a time series of the surface elevation on the sea-swell timescale along the offshore boundary. The phases are selected once using the random phase method and applied to all

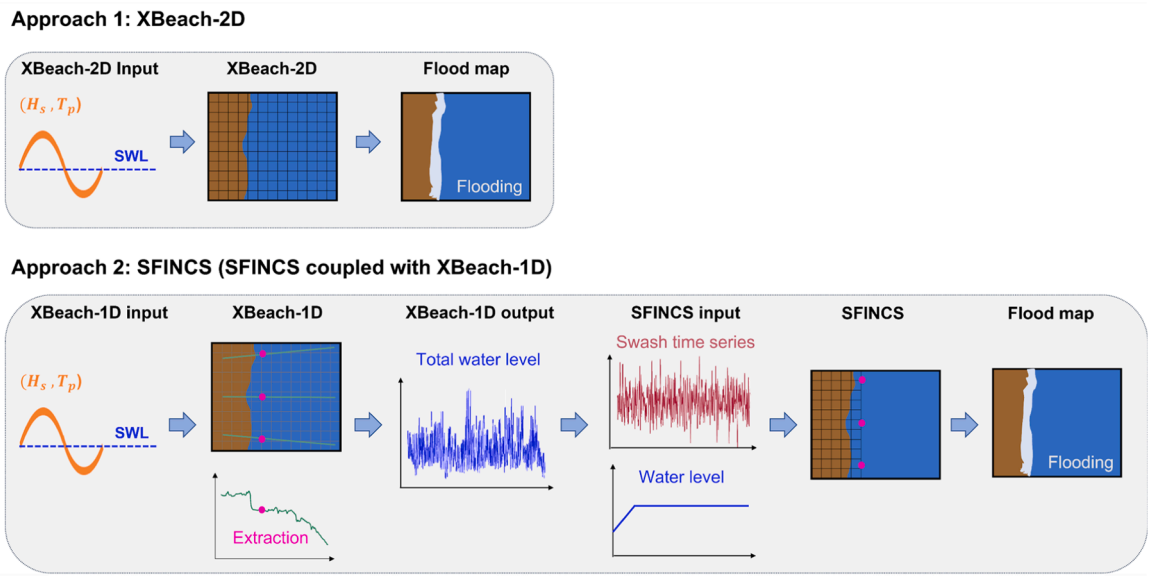

Fig. 2. Diagram detailing the steps of the different flooding approaches compared in this study to assess coastal flooding. The benchmark approach (upper panel) uses the computationally expensive XBeach-2D model. The approach introduced in this study (lower panel) couples the less computationally expensive XBeach-1D model with the super-fast SFINCS flood model. The methodology section describes the coupling of the models in more detail.

components alongshore. This ensures regular phase differences between consecutive wave boundary locations. When using the indirect method, the water levels and the spectra (before calculating the random signal) are smoothed in the longshore direction to overcome large spatial differences.

Coupling (or nesting) XBeach-1D with SFINCS requires finding an optimal depth or coupling location, which can vary between different transects, storm scenarios, sea levels, and geographic areas. The closer to shore the coupling occurs, the more cross-shore evolution of wave-hydrodynamics is resolved within XBeach-1D, allowing a better characterization of shallow water conditions. However, if the coupling location ever becomes dry (water depth becomes zero), numerical instabilities can occur in SFINCS. Further complicating the coupling, local short-wave energy can result in more wave setup than accounted for at the extraction location. A setup correction can be applied to counteract the missed wave setup by increasing the SFINCS input still water level by the difference between the mean water level at the extraction point and the mean water level at a certain minimum water depth (0.1 – 0.5 m) landward of this point.

2.4. Model to model comparison

The skill predictability of the SFINCS flooding approach was assessed based on the differences in flood extents and water depths of flooding with XBeach-2D for every modeled scenario.

We compared flood extents based on the Hit Rate, False Alarm, and Critical Success Index, following Wing et al. (2017). Hit Rate is the ratio between SFINCS flooded cells divided by total flooded cells on the benchmark model (XBeach-2D). This ratio reflects how much SFINCS underpredicts flooding compared to XBeach-2D and ranges from zero (model floods zero of the cells from the benchmark model) to one (both methodologies flood the same grid cells). The False Alarm ratio or False reflects the proportion of flooded cells in SFINCS that are not flooded in XBeach-2D, which is a metric of overestimation. The False value ranges from 0 (no false alarm) to 1 (all false alarms). The Critical Success Index is a metric that matches results in both modeling approaches by factoring in simultaneous underestimation and overestimation values and by ignoring cells that are not flooded in both models. The Success Index has values between 0 (no match between approaches) and 1 (100% match). This study defines a threshold of 10 cm of water depth to define flooding. Thus, every grid cell with a bed elevation higher than 0 m and a water depth equal to or above 10 cm is considered flooded.

For the water depth differences, we used the statistics of mean average difference (MAD), root mean square difference (RMSD), and bias, calculated as:

$$MAD = \frac{1}{n}\sum_{i=1}^{n}\left|x_{i,SFINCS} - x_{i,XBeach2D}\right|$$

$$RMSD = \sqrt{\frac{1}{n}\sum_{i=1}^{n}\left(x_{i,SFINCS} - x_{i,XBeach2D}\right)^2}$$

$$bias = \frac{1}{n}\sum_{i=1}^{n}\left(x_{i,SFINCS} - x_{i,XBeach2D}\right)$$

The water depth differences between models were calculated per grid cell and scenario. MAD indicates the mean difference between models, RMSD is a metric of the model's relative accuracy, and bias reflects the tendency of the SFINCS approach to overestimate (positive value) or underestimate (negative value) the water depth of flooding.

3. Results

3.1. One-dimensional test: finding an optimal coupling methodology and extraction location

To find the optimal coupling methodology and extraction location, we compared the runup computed by SFINCS to XBeach-1D. SFINCS runup results have a bias of underestimating the runup signal compared to XBeach-1D (Fig. 3) when forced directly or indirectly with XBeach-1D outputs. For a 100-yr return period storm and +1.0 m of SLR, the maximum runup is underestimated on average by 12 and 5%, respectively, for the direct and indirect coupling methods. When correcting the indirect method with a wave setup correction calculated at a water depth of 25 cm (SFINCS indirect with setup correction method at 25 cm), it is possible to offset this bias and get a better reproduction of the whole wave runup signal at the cost of overpredicting, on average, 4% of the maximum runup. However, when the setup correction is calculated in shallower waters (SFINCS indirect with setup correction method at 10 cm), the overprediction can increase across the different probabilities of

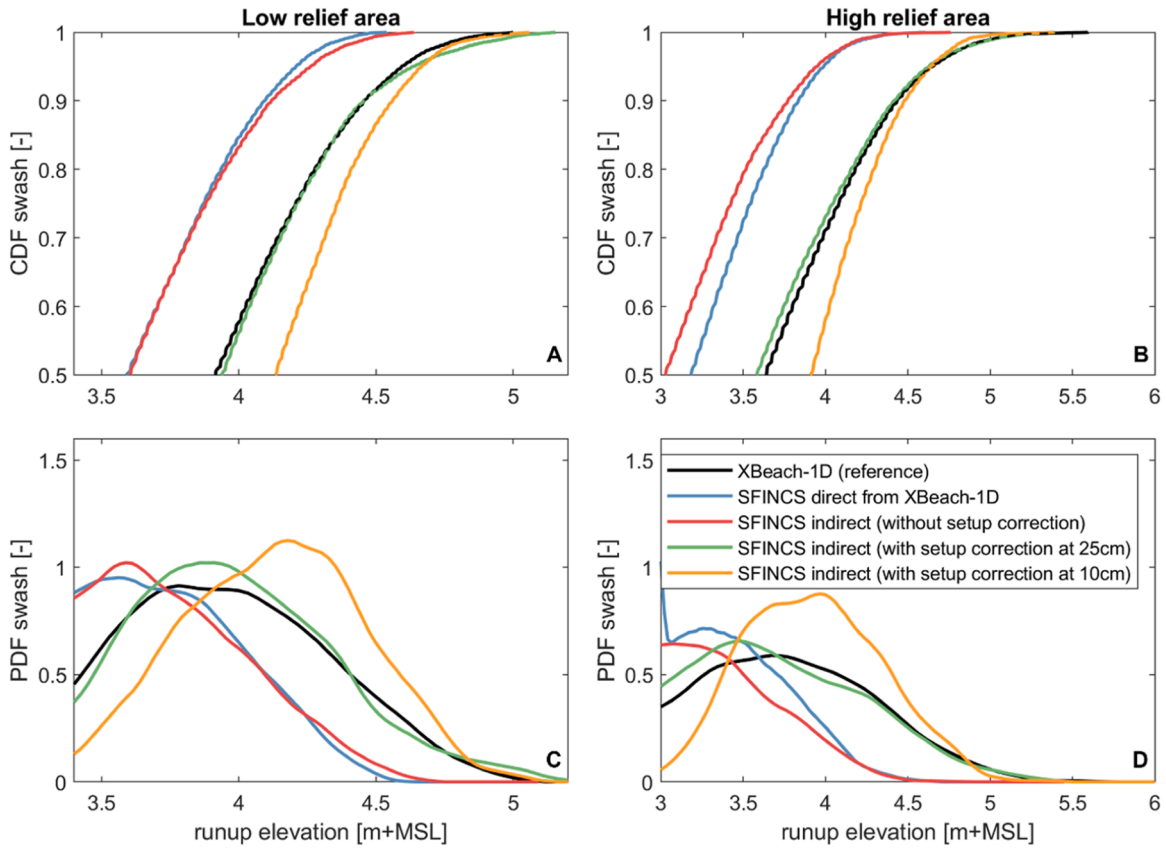

Fig. 3. Cumulative Distribution Function (CDF – A&B) and Probability Density Function (PDF – C&D) of the runup signal for a representative transect of the low relief area (A&C) and the high relief area (B&D) for a 100-yr return period storm and +1.0 m of sea-level rise. The colors represent different methods for coupling XBeach-1D with SFINCS. XBeach-1D outputs can be used directly as SFINCS input (SFINCS direct), or they can be processed to calculate a spectrum-based time series for SFINCS input (SFINCS indirect), which has the option to add a setup correction to account for higher water levels shoreward of the coupling line (SFINCS indirect with setup correction at a water depth of 25 cm and 10 cm). For both areas, the SFINCS indirect method with setup correction calculated at a water depth of 25 cm gives the closest result to the XBeach-1D model runup signal.

runup elevations and shift the runup peak to higher runup elevations. Thus, model results are sensitive to the depth at which the setup correction is calculated, so this depth must be appropriately analyzed and calibrated. For the rest of the analysis, we will use the setup correction calculated at a water depth of 25 cm due to its better representation of the entire runup series, including the peak runup.

SFINCS, directly or indirectly coupled with XBeach-1D, has a clear pattern of increasing skill the closer to shore XBeach-1D outputs are

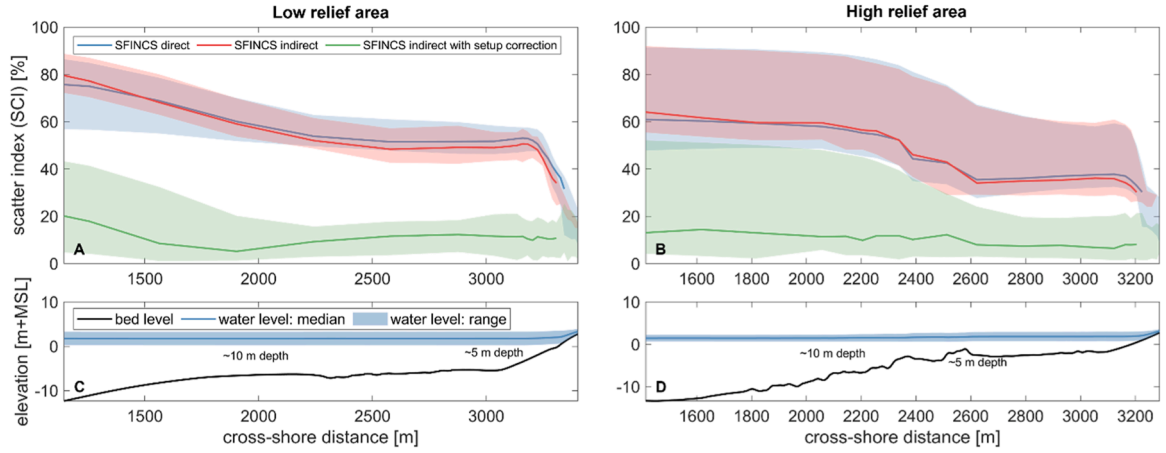

Fig. 4. Runup signal scatter index (SCI) for different coupling methods and extraction locations across the reef for a representative transect of the low relief area (A&C) and the high relief area (B&D). Upper panels (A&B): Scatter Index (SCI) of the SFINCS runup signal compared to XBeach-1D runup signal. SCI is computed for different coupling methods, extraction locations, and modeled scenarios shown in Table 1. Solid lines are the median estimate, and shadings are the 95% confidence interval (CI) range. Different colors are the three different methods for coupling XBeach-1D with SFINCS, as shown in Fig. 3. Lower panels (C&D): transect bed level and mean water level. For both areas, the SFINCS indirect with setup correction coupling method shows a better performance, with the scatter index reaching a stable value lower than 20% for any extraction location shallower than 5 m depth.

extracted (Fig. 4). However, it is possible to extract XBeach-1D deeper in the surf zone and improve the reproductive capabilities of SFINCS by including a setup correction. For example, when including a wave setup correction calculated at a water depth of 25 cm, XBeach-1D results can be extracted at a depth of ~5 m, and the model is able to produce results with an SCI of less than 20% (95% confidence).

The indirect coupling method with setup correction was used to validate the SFINCS flooding approach (XBeach-1D results coupled with SFINCS for 2D flood modeling). The indirect method was selected instead of the direct because it generates a consistent alongshore phasing, which is needed for a 2D application. However, this is a simplification since one would expect phase locking (i.e., a specific ratio between certain frequency components) and a slowly varying alongshore variation of the phase instead of a constant. Secondly, due to its better wave runup reproduction (Fig. 3), we included a setup correction computed at a water depth of 25 cm. Furthermore, the extraction location is defined at the 2 m isobath, which falls in this study's range of high accuracy and has been used in previous efforts coupling wave models with SFINCS (Leijnse et al., 2021).

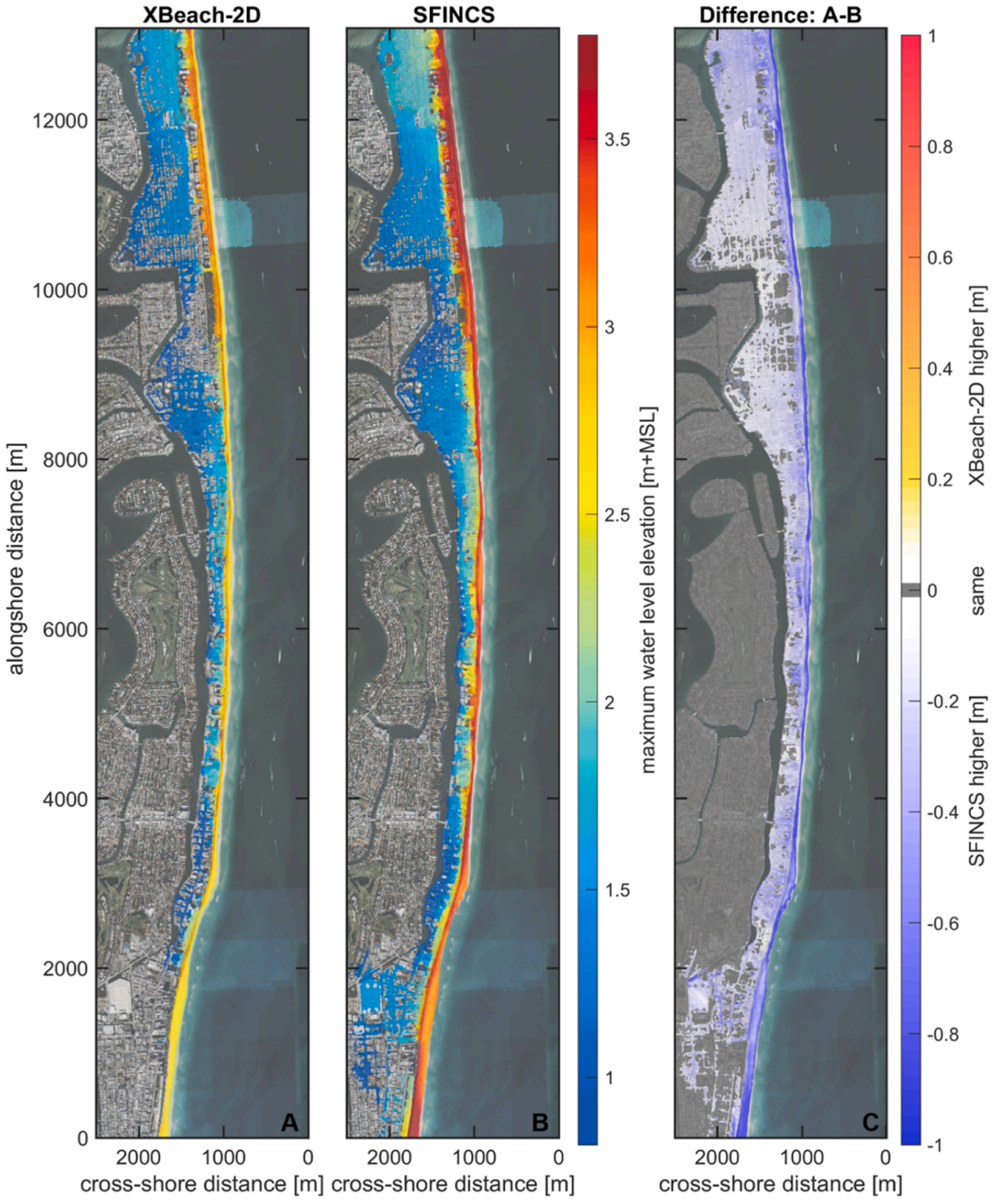

Fig. 5. Comparison of the low relief area flood maps computed with both flooding approaches. Maximum water level elevation computed with XBeach-2D (A), SFINCS forced by XBeach-1D (B), and the difference between both approaches (C). The shown modeled scenario is one of a 100-year return period storm and current sea level. Overall, both flooding approaches generate similar flooding patterns, but the SFINCS approach overestimates flooded areas and water levels. Satellite image extracted from Microsoft Bing Maps.

3.2. Two-dimensional case study: validating the SFINCS flood modeling approach

On the low relief area, the maximum water levels computed with XBeach-2D (Fig. 5A) and the proposed SFINCS flooding approach (Fig. 5B) result in similar flooding patterns, except on the lower part of the map where SFINCS floods a larger area. Water level differences between the models (Fig. 5C) are present across the flood plain. In particular, the proposed SFINCS workflow generally overestimates the nearshore water level. This overestimation is related to the wave setup correction included at the boundary. Overall, the proposed SFINCS method overestimates the surface level and associated flooding with a mean value of 12 cm, which is ~20% of the average flood depth of SFINCS and XBeach-2D.

Due to its steeper topography, a more extreme scenario is shown for the high relief area to allow more flooding (Fig. 6). The SFINCS approach results in similar flood extents to XBeach-2D. However, water level differences are present across the area. Again, there is an overestimation of the nearshore water level (due to the added setup correction), and regions of both flooding underestimation (red colors Fig. 6C) and overestimation (blue colors Fig. 6C) when using the SFINCS approach. Inland waterways and adjacent areas had the largest flood depth and extent underestimations (Fig. 6C). On average, the water levels are overestimated by 3 cm when using SFINCS instead of XBeach-2D, which is ~8% of the average flood depth.

When comparing the flooded area (i.e., flood extent) for all the modeled scenarios, the SFINCS approach underpredicts the flooded area for the less extreme scenarios and overpredicts as the scenarios become more extreme (upper panels Fig. 7). SFINCS overpredicts the flood depth for all the modeled scenarios (lower panels Fig. 7). The models' differences tend to increase with larger waves and storm surges (higher storm return periods) for each SLR scenario. This pattern is more noticeable for the high relief area, where there is a better agreement between models for less extreme and more frequent storms than for more extreme and less frequent ones. The similarity between the models for more extreme scenarios on the low relief area is caused by near total flooding.

The differences between flood depth and extent between the two flooding approaches are larger for the low relief area than for the high relief area. For the low relief area, SFINCS overpredicts, on average, 20% of the flood extent, with a maximum overestimation of 72% and an underestimation of 30%. Meanwhile, in the high relief area, SFINCS, on average, overpredicts 5% of the flood extent, with a maximum overestimation of 26% and an underestimation of 7%. The water depth of flooding is overestimated between 2 and 68% (32% on average) in the low relief area and between 8 and 39% (20% on average) in the high relief area.

SFINCS performance compared to the benchmark model XBeach-2D has different statistical values for the low relief area and high relief area (Fig. 8). Overall, in the low relief area, there are larger flood depth differences between models, with larger standard deviations than the high relief area but fewer outliers. The high relief area has around 8% higher Success Index for flood extent than the low relief area even though the low relief area has a higher Hit Rate (upper panels Fig. 8). This can be explained primarily due to the high relief area having lower False values than the low relief area. Thus, an overall higher underestimation (lower Hit Rate) is compensated by a lower overestimation

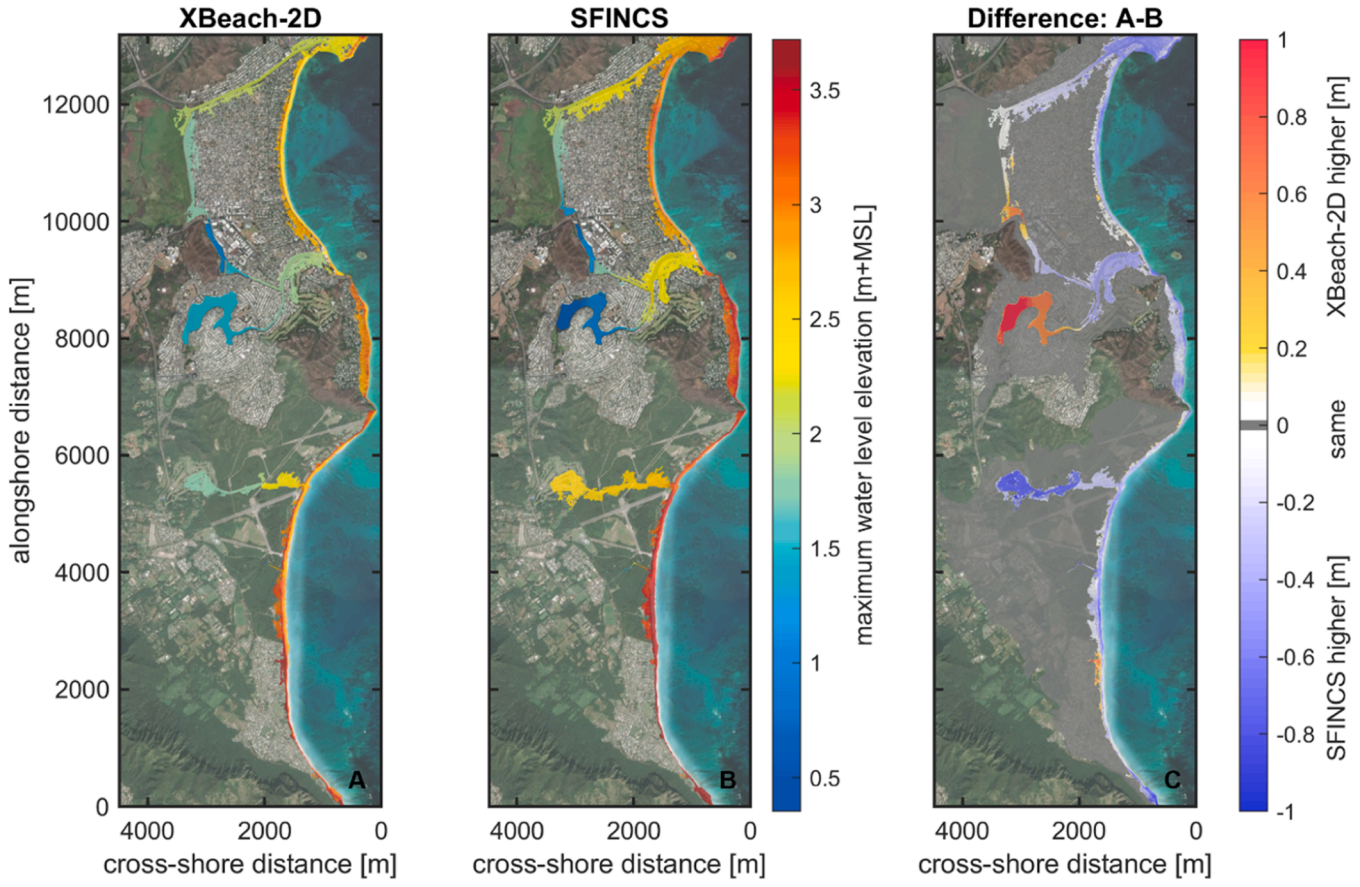

Fig. 6. Comparison of the high relief area flood maps computed with both flooding approaches. Maximum water level elevation computed with XBeach-2D (A), SFINCS forced by XBeach-1D (B), and the difference between both approaches (C). The shown modeled scenario is one of a 100-year return period storm and 1 m sea-level rise. Both flooding approaches generate similar flooding patterns, with an overall overestimation of water levels by the SFINCS approach, except for some inland waterways where XBeach-2D projects higher water levels. Satellite image extracted from Microsoft Bing Maps.

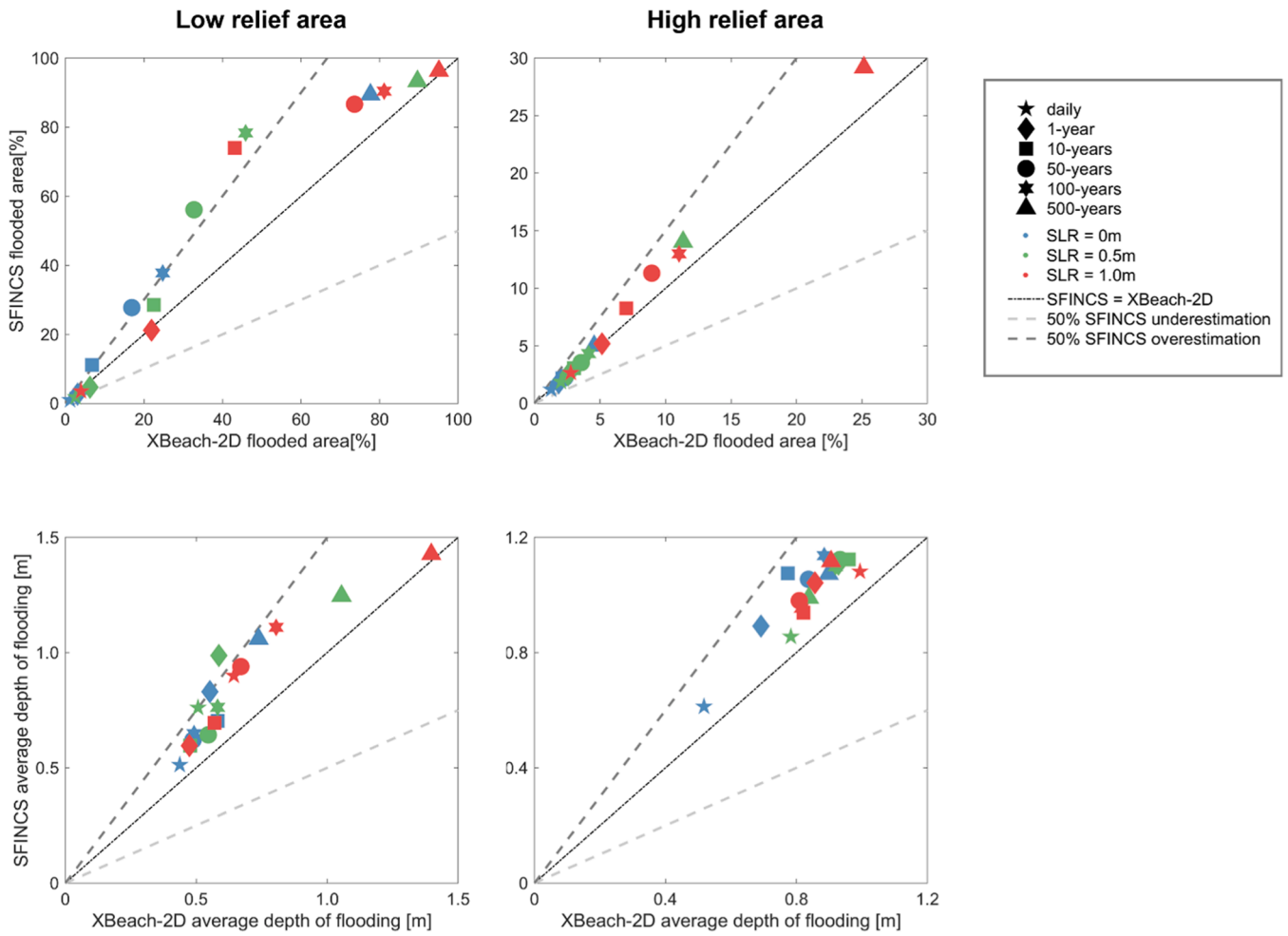

Fig. 7. Comparison of flooding computed with both approaches for all the modeled scenarios in the low relief area (A&C) and the high relief area (B&D). Upper panels (A&B): percentage of the modeled spatial area that is flooded or flood extent. Lower panels (C&D): average water depth of the flooded area. The modeled scenarios include six storm return periods (different markers) across three sea-level rise scenarios (different colors). Markers on the black dash-dotted line (SFINCS = XBeach-2D) mean both models produce the same flooding; above means SFINCS overestimates flooding, and below underestimates flooding compared to XBeach-2D. The dashed lines denote 50% of SFINCS underestimation (light gray) and overestimation (dark gray). Generally, SFINCS overestimates flooding compared to the benchmark XBeach-2D model, with most overestimations being less than 50%.

(lower False). Overall, the SFINCS approach produces flood extents with an accurate performance across scenarios with a low median False between 12–18%, high median Hit Rates between 90–100%, and a high median Success between 78–85%.

Regarding the water depth differences (lower panels Fig. 8), the median MAD, RMSD, and bias are larger for the low relief area than for the high relief area. Both areas present bias values equal to or greater than zero, indicating that the SFINCS flooding method tends to overpredict the flood depth. This overprediction is greater in the low relief area because the water level differences between models are larger at the offshore boundary than in the high relief area, which leads to a lower energy dissipation due to friction when using SFINCS.

A transect analysis was conducted to understand what is driving the flooding overestimation when using the SFINCS approach. Even when reducing the short-wave group variance by 50% (XBeach-1D model parameter *wbcEvarreduce = 0.5)*, XBeach-1D water levels and wave heights are larger than XBeach-2D (Fig. 9). As a result, SFINCS is being forced with larger boundary conditions than XBeach-2D. Close to the extraction point, SFINCS water levels are higher than XBeach-1D due to the added setup correction. As SFINCS does not resolve wave dynamics, the maximum water level decreases inland due to friction, whereas XBeach-1D and XBeach-2D can still add setup after the extraction location due to the presence of short waves (lower panel Fig. 9). Thus, differences between SFINCS and XBeach-2D are higher closer to the offshore boundary and decrease inland.

4. Discussion

We compared the proposed SFINCS flooding approach to XBeach-2D on two contrasting coral reef-lined coastal geomorphologies: a low relief area and a high relief area. This was done to give a range of results inside which most coastlines could be characterized. The proposed flooding approach prioritizes cross-shore processes (e.g., wave shoaling, breaking, and infragravity wave generation) for solving nearshore wave dynamics while neglecting along-shore processes such as diffraction and refraction. Thus, the SFINCS approach is more suitable for environments where cross-shore wave dynamics are the main flooding driver, and it may be subject to higher uncertainty in environments where along-shore processes are dominant (e.g., mild beach coastlines, harbors, headlands, and deep embayments).

Overall, the results of this study indicate that the approach introduced in this paper calculates flooding similarly to XBeach-2D (Fig. 8). However, there are differences between the models' outputs, resulting in both flooding overprediction and underprediction. These differences can be explained by several simplifications applied to the SFINCS approach to make it computationally efficient. The main simplification is using 1D

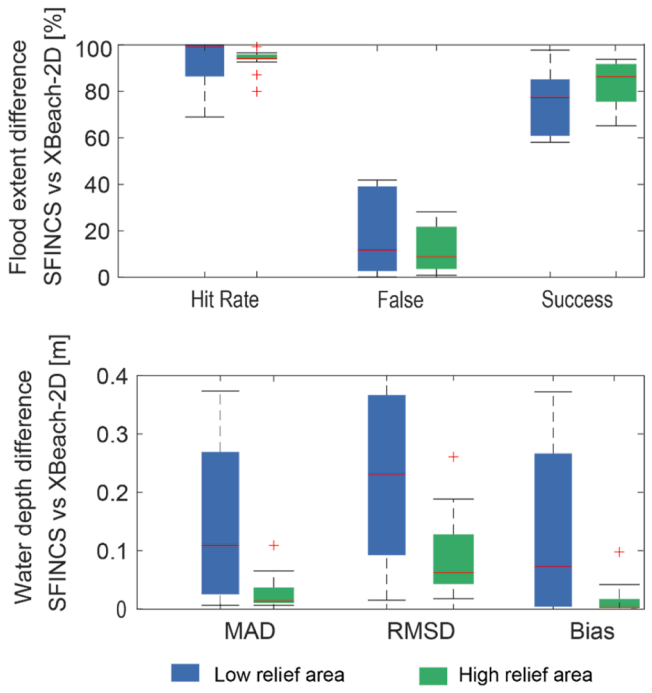

Fig. 8. Flood extent and water depth differences between both modeled flooding approaches for all the simulated scenarios on the low relief area (in blue) and the high relief area (in green). Upper panel: statistical values for flood extent differences (Hit Rate, False, and Success). Lower panel: statistical values for water depth differences (MAD, RMSD, and Bias). Overall, the SFINCS method results show accurate flooding compared to XBeach-2D, with a median Success of around 80% and a median absolute water depth difference of 10 cm or less in both areas.

models that assume alongshore-uniform hydrodynamics and do not include wave directional spreading. Therefore, a runup overprediction is expected due to differences between momentum balances between these two types of modeling. To overcome this difference in the runup and infragravity wave generation, we applied a heuristic reduction on infragravity wave generation at the XBeach boundary with the model parameter *wbcEvarreduce*. We compared wave height values between XBeach-1D and XBeach-2D models between 2 and 0 m isobaths to determine an optimal value to use. However, we made this comparison for the fourth largest storm return periods and did not include SLR scenarios in our analysis. A better assessment would be to compare results for the lowest and highest return period storms and SLR. The comparison should consist of both nearshore wave heights and mean water levels for a more comprehensive calibration of this model parameter value.

Another main simplification is applying a setup correction to compensate for using a simplified physics model such as SFINCS. As this model does not solve radiation stress, these wave dynamics must be solved within XBeach-1D and offshore of the coupling line (i.e., 2 m isobath). However, as we study a wide range of storm and SLR conditions, wave breaking can still occur onshore of the coupling line, which generates a wave setup that can lead to a higher mean water level than the one calculated at the coupling line. To compensate for this mismatch, a setup correction, calculated at a water depth of 25 cm, was added to the SFINCS boundary conditions to reproduce a similar runup signal to the XBeach-1D transects (Fig. 3). The setup correction approach has the caveat of having, on average, a maximum runup overestimation of 4% (Fig. 3) and a SCI in the runup signal of 20% (Fig. 4), which can lead to some flooding overprediction in the nearshore (Figs. 5 and 6). However, it can also help compensate for some underprediction in flooding from the SFINCS approach, mainly occurring on inland waterways and surrounding areas (Fig. 6). This underprediction happens because the remaining high-frequency sea-swell waves close to shore (lower panel Fig. 9) continue propagating inland, as demonstrated when using the more complete XBeach-2D. However, these high-frequency waves are not accounted for in SFINCS boundary conditions. Therefore, SFINCS tends to underestimate flooding in inland waterways when high-frequency waves have not yet been largely dissipated.

To better understand uncertainties arising from our proposed

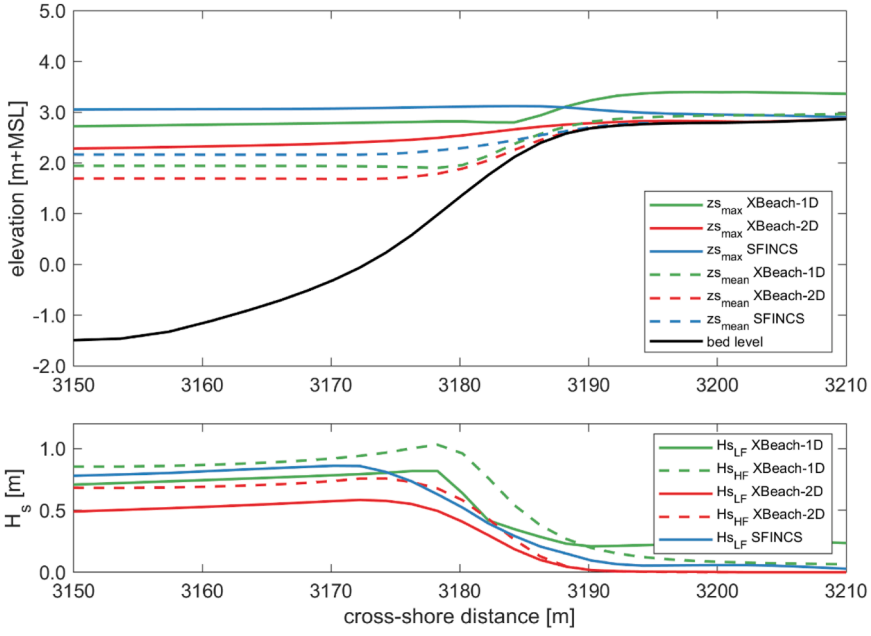

Fig. 9. Water level and wave height comparison between all the hydrodynamics models used in this study on a high relief area representative transect. The scenario shown is a 500-year return period storm and current sea level. Upper panel: maximum water levels (zs_{max}) and mean water levels (zs_{mean}). Lower panel: short wave significant wave height (HS_{HF}) and infragravity wave significant wave height (HS_{LF}). Water levels and wave heights are higher in XBeach-1D and SFINCS models than in XBeach-2D.

approach, we also forced SFINCS with water level time series extracted from XBeach-2D at the coupling line (i.e., 2 m isobath). We used the indirect method for the same scenarios modeled in Figs. 5 and 6 and did not apply a setup correction. We found that when forced with XBeach-2D outputs, SFINCS tends to underpredict flooding (not shown). The water depth of flooding was underpredicted on average by 9 cm in the low relief area and 5 cm in the high relief area. When forced with data extracted at the 1 m isobath, the underestimation decreases slightly (~1%) in both areas. We hypothesize that this underestimation is driven by missing the water level increase due to the setup generated by waves breaking onshore of the coupling line. These tests restate the importance of extracting the data where relevant hydrodynamics have been solved. However, as previously mentioned, this optimal extraction location varies depending on the boundary conditions and the bathymetry (Fig. 4) and is thus unknown a priori. Using the proposed methodology that relies on 1D models, these effects can be partially counterbalanced with the setup correction.

Flooding differences between the modeling approaches can be reduced when more numerical parameters are calibrated per site. For example, in regions with a complex relief and different infragravity wave contributions to flooding, the correction of the incoming infragravity wave generation (model parameter *wbcEvarreduce*) can be adjusted in XBeach-1D models to reproduce the generation of infragravity waves more accurately. Particularly in our study, we found that flooding differences between SFINCS and XBeach-2D are higher in the low relief area than in the high relief area. The latter can be partially explained because the low relief area needs at least ~25% more infragravity wave generation reduction than the 50% we accounted for in our study. For example, when reducing the infragravity wave generation by 75% in the low relief area for the same scenario as Fig. 5, the average water depth of flooding difference between models was reduced by 25% compared to when using 50% of wave energy reduction. The water level differences in the nearshore decreased, and the flood extent became more similar (not shown), especially in the lower part of Fig. 5, where more of the overestimated flood extent occurred. On the other hand, when applying a 75% infragravity wave generation reduction in the high relief area for the same scenario as Fig. 6, the average water depth of flooding difference decreased by 66% compared to when using a 50% wave energy reduction. However, larger areas of flooding underestimation could be found close to the coastline and inland waterways (not shown). Furthermore, the flood extent and water depth of flooding were overestimated when the XBeach-1D infragravity wave generation was not reduced. The overestimation of the water depth of flooding increased on average by 17% in the low relief area and 73% in the high relief area. These differences highlighted the relevance of calibrating these models per specific site. For new projects, it is advised to carry out a site calibration by selecting a short representative coast stretch and compare the proposed SFINCS flooding method with a fully resolving 2D model (e.g., XBeach-2D) for a range of *wbcEvarreduce* values and boundary conditions.

Additionally, the SFINCS flooding accuracy can be improved by adjusting the minimum depth defined to account for the setup correction. For example, the SFINCS approach in the low relief area gave slightly more accurate results when the setup correction was calculated based on 50 cm water depth instead of the 25 cm obtained for the high relief area (not shown). The selected water depth to account for extra setup can increase or decrease the maximum runup height and shift the runup peak compared to XBeach-1D results (Fig. 3). Thus, for future projects, it is advised to carry out a site calibration by selecting representative transects and developing an analysis similar to Fig. 3. It is recommended to calibrate the model for the endmembers of the 1D models wave climate and water level boundary conditions. An extra step for calibration would be to calibrate SFINCS bottom friction values by comparing results between SFINCS forced with XBeach-1D and XBeach-2D outputs.

Even though additional steps are needed to couple SFINCS with XBeach-1D outputs (Fig. 2), the computational cost is on the order of 100 times faster than when using XBeach-2D. For one scenario, XBeach-2D takes ~11 days to run in parallel using the whole capacity of a 32-logical processor computer with 48 GB RAM, and the SFINCS approach takes ~0.1 days (~1–1.5 h) when running ~30 XBeach-1D in series and SFINCS using total capacity. This efficiency is based on 1) the efficiency of SFINCS in solving overland flooding and 2) only resolving wave hydrodynamics on transects. The savings in computational cost make the proposed flooding approach especially suitable for large-scale areas and regional models where flooding needs to account for wave-driven processes, and several XBeach-2D models would be required to cover the project area. XBeach-2D would be more applicable for modeling small-scale projects requiring higher accuracy. Although the initial effort needed to build the SFINCS model can be time-consuming, primarily due to the manual editing of the coupling line, this effort only needs to be done once when the extraction location is selected shallower than 5 m of water depth and the setup correction is included in the boundary conditions (Fig. 4). In that case, the same SFINCS setup can be used for a wide range of wave climate and sea level rise scenarios, and only the SFINCS boundary conditions need to be adjusted per scenario. Therefore, the proposed flooding approach using SFINCS can save considerable computational expense, allowing the simulation of more scenarios or larger geographical domains.

Future steps should focus on continued model validation. First, non-hydrostatic models (that resolve short and infragravity waves) have been found to better represent more frequent storms compared to hydrostatic models (Quataert et al., 2020). These models could help to better represent flood extents caused by low return period storms and low SLR scenarios, which were generally underestimated in our study (Fig. 7). Thus, evaluating discrepancies between models is crucial to understanding their accuracy. We envision exploring the range of boundary conditions under which the SFINCS method may benefit from using non-hydrostatic models as a source of boundary conditions. Second, validating the proposed flooding approach with observations in addition to wave models is essential to assess its uncertainties. Such validations will also help calibrate and improve the SFINCS approach, which could be used for other applications such as global modeling, different ecosystems modeling, and early warning systems.

5. Conclusions

In this study, we introduced and validated, against XBeach-2D, an improved physics-based and computationally efficient approach, SFINCS coupled with XBeach-1D, to assess regional wave-driven flooding on reef-lined coastlines. Different coupling methodologies were tested, and it was found that coupling SFINCS with XBeach-1D using an indirect coupling method (i.e., spectra-based with constant phase difference) and adding a setup correction ('SFINCS indirect with setup correction') gives an accurate runup reproduction compared to XBeach-1D results. When using this method and coupling the models at a water depth of less than 5 m, the scatter index for wave runup is contained under 20% across modeled wave climate scenarios and geographies.

The proposed flooding approach yields a similar flooding extent compared to XBeach-2D, flooding on average 92% of the same cells (Hit Rate). However, weaker, high-frequency storm flood extents tend to be underpredicted (maximum of 7% for the high relief area and 30% for the low relief area). In contrast, stronger, low-frequency storm flood extents are overpredicted (maximum of 26% for the high relief area and 70% for the low relief area). The predicted water depth of flooding generally exhibits an overestimation across scenarios, with a positive bias of 7 cm, an MAE of 9 cm, and an RMSD of 15 cm.

The proposed method offers a 100 times the computational speed-up compared to XBeach-2D. This makes it a suitable choice for large-scale flood modeling involving numerous scenarios, particularly in regions where wave-driven flooding is the primary concern due to the model's emphasis on cross-shore wave processes.

CRediT authorship contribution statement

Camila Gaido-Lasserre: Conceptualization, Methodology, Software, Validation, Visualization, Writing – original draft, Writing – review & editing. **Kees Nederhoff:** Conceptualization, Methodology, Software, Validation, Visualization, Writing – review & editing. **Curt D. Storlazzi:** Conceptualization, Funding acquisition, Supervision, Writing – review & editing. **Borja G. Reguero:** Funding acquisition, Supervision, Writing – review & editing. **Michael W. Beck:** Funding acquisition, Supervision, Writing – review & editing.

Declaration of competing interest

The authors declare that they have no known competing financial interests or personal relationships that could have appeared to influence the work reported in this paper.

Data availability

The model setup and data for this research can be found at https://doi.org/10.5281/zenodo.10805614.

Acknowledgments

This research was financially supported by the U.S. Department of Interior, U.S. Geological Survey through the Coastal and Marine Hazards and Resources Program. CGL was supported in part by the UCSC Center for Coastal Climate Resilience. MWB was supported in part by an AXA Research Chair and the UCSC Center for Coastal Climate Resilience. BGR acknowledges the support from an Early-Career Research Fellowship from the Gulf Research Program of the National Academies of Sciences, Engineering, and Medicine, although the content is the responsibility of the authors and does not necessarily represent the official views of the Gulf Research Program of the National Academy of Sciences, Engineering and Medicine. This article has been peer reviewed and approved for publication consistent with USGS Fundamental Science Practices (https://pubs.usgs.gov/circ/1367/). Anita Engelstad (USGS) provided a timely review of our work. Any use of trade, firm, or product names is for descriptive purposes only and does not imply endorsement by the U.S. Government.

Appendix

XBeach-1D (params.txt file)

%%% Flow boundary condition parameters front = abs_1d left = wall right = wall back = abs_1d

%%% Flow parameters bedfriction = manning bedfricfile = bedfricfile.txt

%%% General avalanching = 0 fwfile = fwfile.txt rotate = 0 wbcEvarreduce = 0.500000

%%% Grid parameters depfile = bed.dep posdwn = −1 nx = 1802 ny = 0 vardx = 1 dy = 0 xfile = *x*.grd yfile = *y*.grd xori = 0 yori = 0 thetamin = 0 thetamax = 360 dtheta = 360

%%% Model time tstop = 23,400

%%% Physical processes sedtrans = 0 morphology = 0

%%% Tide boundary conditions zs0file = tide.txt tideloc = 1

%%% Wave boundary condition parameters instat = jons

%%% Wave-spectrum boundary condition parameters bcfile = jonswap.txt rt = 25,560

%%% Output variables outputformat = netcdf rugdepth = 0.020000 tintm = 7200 tintp = 0.500000 tintg = 3600 tstart = 100 nglobalvar = 7

H zs zb

E urms taubx tauby nmeanvar = 6

H zs zb urms taubx tauby npointvar = 5 zb zs u

H v npoints = 3

631,036.07 2370,336.87

630,993.39 2370,350.00

630,962.09 2370,359.63 nrugauge = 1

630,948.7066 2370,363.7511

SFINCS (sfincs.inp file)

mmax = 1320 nmax = 2241 dx = 10 dy = 2 x0 = 637,638.4588 y0 = 2358,950.8301 rotation = 120 latitude = 0 tref = 20,100,101 000,000 tstart = 20,100,101 000,000 tstop = 20,100,101 074,400 tspinup = 60 dtmapout = 3600 dthisout = 1 dtmaxout = 3600 dtwnd = 3600 alpha = 0.5 theta = 0.8 huthresh = 0.005 manning = 0.04 manning_land = 0.035 manning_sea = 0.02 rgh_lev_land = 0 zsini = 0 qinf = 0 rhoa = 1.25 rhow = 1024 dtmax = 999 maxlev = 999 bndtype = 1 advection = 2 baro = 0 pavbnd = 0 gapres = 101,200 advlim = 5 stopdepth = 100 depfile = sfincs.dep mskfile = sfincs.msk indexfile = sfincs.ind bndfile = sfincs.bnd obsfile = sfincs.obs inputformat = bin outputformat = net cdnrb = 3 cdwnd = 0 28 50 cdval = 0.001 0.0025 0.0015 geomskfile = sfincs.gms dtout = 3600 min_lev_hmax = −10 netbndbzsbzifile= sfincs_netbndbzsbzifile.nc bzifile = dummy

XBeach-2D (params.txt file)

%%% Flow parameters bedfriction = manning bedfricfile = bedfricfile.txt

%%% General dtheta_*s* = 10 fwfile = fwfile.txt nspectrumloc = 132 rotate = 0 single_dir = 1 vegetation = 0 wavemodel = surfbeat

%%% Grid parameters depfile = bed.dep posdwn = −1 nx = 2826 ny = 1319 alfa = 0 vardx = 1 xfile = *x*.grd yfile = *y*.grd xori = 0 yori = 0 thetamin = 0 thetamax = 360 dtheta = 360 thetanaut = 1

%%% Model time tstop = 27,480

%%% Physical processes sedtrans = 0 morphology = 0

%%% Tide boundary conditions zs0file = tide.txt tideloc = 1

%%% Wave boundary condition parameters instat = jons

%%% Wave numerics parameters maxiter = 1000

%%% Wave-spectrum boundary condition parameters bcfile = loclist.txt rt = 27,481

%%% Output variables outputformat = netcdf tintm = 3600 tintg = 1800 nglobalvar = 5 zs zb u v H

nmeanvar = 5 zs zb u v H

npointvar = 5 zs zb u v

References

Anderson, M., 2007. Benthic Habitats of the Main Eight Hawaiian Islands Derived from IKONOS and Quick Bird Satellite Imagery, 2004–2006. Analytical Laboratories of Hawaii. https://products.coastalscience.noaa.gov/collections/benthic/e97hawaii/data2007.aspx.

Armaroli, C., Duo, E., Viavattene, C., 2019. From hazard to consequences: evaluation of direct and indirect impacts of flooding along the Emilia-Romagna Coastline, Italy. Front. Earth Sci. 7 (August), 1–20. https://doi.org/10.3389/feart.2019.00203.

Barnard, P.L., Erikson, L.H., Foxgrover, A.C., Hart, J.A.F., Limber, P., O'Neill, A.C., van Ormondt, M., Vitousek, S., Wood, N., Hayden, M.K., Jones, J.M., 2019. Dynamic flood modeling essential to assess the coastal impacts of climate change. Sci. Rep. 9 (1), 1–13. https://doi.org/10.1038/s41598-019-40742-z.

Bates, P.D., Dawson, R.J., Hall, J.W., Horritt, M.S., Nicholls, R.J., Wicks, J., Ali Mohamed Hassan, M.A., 2005. Simplified two-dimensional numerical modelling of coastal flooding and example applications. Coastal Eng. 52 (9), 793–810. https://doi.org/10.1016/j.coastaleng.2005.06.001.

Betancourt, J., Bachoc, F., Klein, T., Idier, D., Pedreros, R., Rohmer, J., 2020. Gaussian process metamodeling of functional-input code for coastal flood hazard assessment. Reliab. Eng. Syst. Saf. 198, 106870 https://doi.org/10.1016/j.ress.2020.106870. November 2019.

Booij, N., Ris, R.C., Holthuijsen, L.H., 1999. A third-generation wave model for coastal regions 1. Model description and validation. J. Geophys. Res. Oceans 104 (C4), 7649–7666. https://doi.org/10.1029/98JC02622.

Camus, P., Méndez, F.J., Losada, I.J., Menéndez, M., Espejo, A., Pérez, J., 2014. A method for finding the optimal predictor indices for local wave climate conditions. Ocean Dyn. 1025–1038. https://doi.org/10.1007/s10236-014-0737-2.

Camus, P., Mendez, F.J., Medina, R., 2011. A hybrid efficient method to downscale wave climate to coastal areas. Coast. Eng. 58 (9), 851–862. https://doi.org/10.1016/j.coastaleng.2011.05.007.

Carignan, K.S., McLean, S.J., Eakins, B.W., Beasley, L., Love, M.R., Sutherland, M., 2015. Miami 1/3 Arc-Second MHW Coastal Digital Elevation Model. National Oceanic and Atmospheric Administration. https://data.noaa.gov//metaview/page?xml=NOAA/NESDIS/NGDC/MGG/DEM/iso/xml/5270.xml&view=getDataView&header=none.

Cheriton, O.M., Storlazzi, C.D., Rosenberger, K.J., 2016. Observations of wave transformation over a fringing coral reef and the importance of low-frequency waves and offshore water levels to runup, overwash, and coastal flooding. J. Geophys. Res. Oceans 121. https://doi.org/10.1002/2015JC011231.

Eilander, D., Couasnon, A., Leijnse, T., Ikeuchi, H., Yamazaki, D., Muis, S., Dullaart, J., Haag, A., Winsemius, H.C., Ward, P.J., 2023. A globally applicable framework for compound flood hazard modeling. Nat. Hazards Earth Syst. Sci. 23 (2), 823–846. https://doi.org/10.5194/nhess-23-823-2023.

Ferrario, F., Beck, M.W., Storlazzi, C.D., Micheli, F., Shepard, C.C., Airoldi, L., 2014. The effectiveness of coral reefs for coastal hazard risk reduction and adaptation. Nat. Commun. 5 (May), 1–9. https://doi.org/10.1038/ncomms4794.

Florida Fish and Wildlife Conservation Commission–Fish and Wildlife Research Institute, 2016. Unified Florida Coral Reef Tract Map Version 2.0. Florida Fish and Wildlife Conservation Commission–Fish and Wildlife Research Institute. http://ocean.floridamarine.org/IntegratedReefMap/UnifiedReefTract.htm.

Gouldby, B., Méndez, F.J., Guanche, Y., Rueda, A., Mínguez, R., 2014. A methodology for deriving extreme nearshore sea conditions for structural design and flood risk analysis. Coast. Eng. 88, 15–26. https://doi.org/10.1016/j.coastaleng.2014.01.012.

Guza, R.T., Feddersen, F., 2012. Effect of wave frequency and directional spread on shoreline runup. Geophys. Res. Lett. 39 (11), 1–5. https://doi.org/10.1029/2012GL051959.

Guza, R.T., Thornton, E.B., Holman, R.A., 1984. Swash on steep and shallow beaches. In: Proceedings of the Coastal Engineering. American Society of Civil Engineers, New York, pp. 708–723. https://doi.org/10.9753/icce.v19.48 (Houston, U.S.A.: Sep. 3-7, 1984)pages.

Hardy, T.A., Young, I.R., 1996. Field study of wave attenuation on an offshore coral reef. J. Geophys. Res. Oceans 101 (C6), 14311–14326. https://doi.org/10.1029/96JC00202.

Hasselmann, K., Barnett, T.P., Bouws, E., Carlson, H., Cartwright, D.E., Eake, K., Euring, J.A., Gicnapp, A., Hasselmann, D.E., Kruseman, P., Meerburg, A., Mullen, P., Olbers, D.J., Richren, K., Sell, W., & Walden, H. (1973). Measurements of Wind-Wave Growth and Swell Decay During the Joint North Sea Wave Project (JONSWAP). January.

Hoeke, R., Storlazzi, C., Ridd, P., 2011. Hydrodynamics of a bathymetrically complex fringing coral reef embayment: wave climate, *in situ* observations, and wave prediction. J. Geophys. Res. Oceans 116 (4), 1–19. https://doi.org/10.1029/2010JC006170.

Idier, D., Aurouet, A., Bachoc, F., Baills, A., Betancourt, J., Gamboa, F., Klein, T., López-Lopera, A.F., Pedreros, R., Rohmer, J., Thibault, A., 2021. A user-oriented local coastal flooding early warning system using metamodelling techniques. J. Mar. Sci. Eng. 9 (11) https://doi.org/10.3390/jmse9111191.

Jamieson, S., Lhomme, J., Wright, G., Gouldby, B., 2012. A highly efficient 2D flood modelling with sub-element topography. Proc. Ice Water Manag. 165 (10), 581–595. https://doi.org/10.1680/wama.12.00021.

Kernkamp, H.W.J., Van Dam, A., Stelling, G.S., De Goede, E.D., 2011. Efficient scheme for the shallow water equations on unstructured grids with application to the Continental Shelf. Ocean Dyn. 61 (8), 1175–1188. https://doi.org/10.1007/s10236-011-0423-6.

Lashley, C.H., Roelvink, D., van Dongeren, A., Buckley, M.L., Lowe, R.J., 2018. Nonhydrostatic and surfbeat model predictions of extreme wave run-up in fringing reef environments. Coast. Eng. 137 (February), 11–27. https://doi.org/10.1016/j.coastaleng.2018.03.007.

Leijnse, T., van Ormondt, M., Nederhoff, K., van Dongeren, A., 2021. Modeling compound flooding in coastal systems using a computationally efficient reduced-physics solver: including fluvial, pluvial, tidal, wind- and wave-driven processes. Coast. Eng. 163, 103796 https://doi.org/10.1016/j.coastaleng.2020.103796. July 2020.

Love, M.R., Friday, D.Z., Grothe, P.R., Lim, E., Carignan, K.S., Eakins, B.W., and Taylor, L.A. (n.d.). Oahu, Hawaii 1/3 Arc-Second MHW Coastal Digital Elevation Model: National Oceanic and Atmospheric Administration. Retrieved March 1, 2019, from https://data.noaa.gov//metaview/page?xml=NOAA/NESDIS/NGDC/MGG/DEM/iso/xml/3410.xml&view=getDataView&header=none.

Lowe, R.J., Falter, J.L., Monismith, S.G., Atkinson, M.J., 2009. A numerical study of circulation in a coastal reef-lagoon system. J. Geophys. Res. Oceans 114 (6), 1–18. https://doi.org/10.1029/2008JC005081.

Luettich, R.A., Westerink, J.J., Scheffner, N.W., 1992. ADCIRC: An Advanced Three-Dimensional Circulation Model for Shelves Coasts and Estuaries, Report 1: Theory and Methodology of ADCIRC-2DDI and ADCIRC-3DL, Dredging Research Program Technical Report DRP-92-6. Coastal Engineering Research Center (U.S.). E. https://erdc-library.erdc.dren.mil/jspui/handle/11681/4618.

McCall, R., Van Santen, R., Wilmink, R., De Bakker, A., Steetzel, H., Pluis, S., De Ridder, M., Coumou, L., Van Kuik, N., 2023. Accounting for directional wave spreading effects on infragravity wave growth in a 1D dune erosion model. In: Proceedings of the Coastal Sediments 2023.

NOAA, 2020. Extreme Water Levels–Annual Exceedance Probability Curves. NOAA. Retrieved March 1from. https://tidesandcurrents.noaa.gov/est/.

Nwogu, O., Demirbilek, Z., 2010. Infragravity wave motions and runup over shallow fringing reefs. J. Waterw. Port Coast. Ocean Eng. 136 (6), 295–305. https://doi.org/10.1061/(asce)ww.1943-5460.0000050.

Péquignet, A.C., Becker, J.M., Merrifield, M.A., Boc, S.J., 2011. The dissipation of wind wave energy across a fringing reef at Ipan, Guam. Coral Reefs 30 (1), 71–82. https://doi.org/10.1007/s00338-011-0719-5. SUPPL.

Péquignet, A.C.N., Becker, J.M., Merrifield, M.A., Aucan, J., 2009. Forcing of resonant modes on a fringing reef during tropical storm Man-Yi. Geophys. Res. Lett. 36 (3), 20–23. https://doi.org/10.1029/2008GL036259.

Quataert, E., Storlazzi, C., Van Rooijen, A., Cheriton, O., Van Dongeren, A., 2015. The influence of coral reefs and climate change on wave-driven flooding of tropical coastlines. Geophys. Res. Lett. 42 (15), 6407–6415. https://doi.org/10.1002/2015GL064861.

Quataert, E., Storlazzi, C., van Dongeren, A., McCall, R., 2020. The importance of explicitly modelling sea-swell waves for runup on reef-lined coasts. Coastal Eng. 160 (April), 103704. doi:10.1016/j.coastaleng.2020.103704.

Reguero, B.G., Menéndez, M., Méndez, F.J., Mínguez, R., Losada, I.J., 2012. A Global Ocean Wave (GOW) calibrated reanalysis from 1948 onwards. Coast. Eng. 65, 38–55. https://doi.org/10.1016/j.coastaleng.2012.03.003.

Reguero, B.G., Storlazzi, C.D., Gibbs, A.E., Shope, J.B., Cole, A.D., Cumming, K.A., Beck, M.W., 2021. The value of US coral reefs for flood risk reduction. Nat. Sustain. 4 (8), 688–698. https://doi.org/10.1038/s41893-021-00706-6.

Roeber, V., Bricker, J.D., 2015. Destructive tsunami-like wave generated by surf beat over a coral reef during Typhoon Haiyan. Nat. Commun. 6, 1–9. https://doi.org/10.1038/ncomms8854.

Roelvink, D., McCall, R., Mehvar, S., Nederhoff, K., Dastgheib, A., 2018. Improving predictions of swash dynamics in XBeach: the role of groupiness and incident-band runup. Coast. Eng. 134, 103–123. https://doi.org/10.1016/j.coastaleng.2017.07.004. July 2017.

Roelvink, D., Reniers, A., van Dongeren, A., van Thiel de Vries, J., McCall, R., Lescinski, J., 2009. Modelling storm impacts on beaches, dunes and barrier islands. Coast. Eng. 56 (11–12), 1133–1152. https://doi.org/10.1016/j.coastaleng.2009.08.006.

Rohmer, J., Idier, D., 2012. A meta-modelling strategy to identify the critical offshore conditions for coastal flooding. Nat. Hazards Earth Syst. Sci. 12 (9), 2943–2955. https://doi.org/10.5194/nhess-12-2943-2012.

Rueda, A., Cagigal, L., Pearson, S., Antolínez, J.A.A., Storlazzi, C., van Dongeren, A., Camus, P., Mendez, F.J., 2019a. HyCReWW: a hybrid coral reef wave and water level metamodel. Comput. Geosci. 127, 85–90. https://doi.org/10.1016/j.cageo.2019.03.004.

Rueda, A., Cagigal, L., Pearson, S., Antolínez, J.A.A., Storlazzi, C., van Dongeren, A., Camus, P., Mendez, F.J., 2019b. HyCReWW: a hybrid coral reef wave and water level metamodel. Comput. Geosci. 127, 85–90. https://doi.org/10.1016/j.cageo.2019.03.004. February 2018.

Sebastian, A., Bader, D.J., Nederhoff, C.M., Leijnse, T.W.B., Bricker, J.D., Aarninkhof, S.G.J., 2021. Hindcast of pluvial, fluvial, and coastal flood damage in Houston, Texas during Hurricane Harvey (2017) using SFINCS. Nat. Hazards 109 (3), 2343–2362. https://doi.org/10.1007/s11069-021-04922-3.

Sheppard, C., Dixon, D.J., Gourlay, M., Sheppard, A., Payet, R., 2005. Coral mortality increases wave energy reaching shores protected by reef flats: examples from the Seychelles. Estuar. Coast. Shelf Sci. 64 (2–3), 223–234. https://doi.org/10.1016/j.ecss.2005.02.016.

Shi, F., Kirby, J.T., Harris, J.C., Geiman, J.D., Grilli, S.T., 2012. A high-order adaptive time-stepping TVD solver for Boussinesq modeling of breaking waves and coastal inundation. Ocean Model. 36–51. https://doi.org/10.1016/j.ocemod.2011.12.004, 43–44.

Shimozono, T., Tajima, Y., Kennedy, A.B., Nobuoka, H., Sasaki, J., Sato, S., 2015. Combined infragravity wave and sea-swell runup over fringing reefs by super typhoon Haiyan. J. Geophys. Res. Oceans 120. https://doi.org/10.1002/2015JC010760.

Storlazzi, C.D., Elias, E.P.L., Berkowitz, P., 2015. Many atolls may be uninhabitable within decades due to climate change. Sci. Rep. 5, 1–9. https://doi.org/10.1038/srep14546.

Storlazzi, C.D., Gingerich, S.B., Van Dongeren, A., Cheriton, O.M., Swarzenski, P.W., Quataert, E., Voss, C.I., Field, D.W., Annamalai, H., Piniak, G.A., McCall, R., 2018. Most atolls will be uninhabitable by the mid-21st century because of sea-level rise exacerbating wave-driven flooding. Sci. Adv. 4 (4), 1–10. https://doi.org/10.1126/sciadv.aap9741.

Storlazzi, C.D., Reguero, B.G., Cole, A.D., Lowe, E., Shope, J.B., Gibbs, A.E., Nickel, B.A., McCall, R.T., van Dongeren, A.R., & Beck, M.W. (2019). Rigorously Valuing the Role of U.S. Coral Reefs in Coastal Hazard Risk Reduction. USGS Open-File Report 2019-1027, 42. https://pubs.er.usgs.gov/publication/ofr20191027.

Taherkhani, M., Vitousek, S., Barnard, P.L., Frazer, N., Anderson, T.R., Fletcher, C.H., 2020. Sea-level rise exponentially increases coastal flood frequency. Sci. Rep. 10 (1), 1–17. https://doi.org/10.1038/s41598-020-62188-4.

Toimil, A., Álvarez-Cuesta, M., Losada, I.J., 2023. Neglecting the effect of long- and short-term erosion can lead to spurious coastal flood risk projections and maladaptation. Coast. Eng. 179 https://doi.org/10.1016/j.coastaleng.2022.104248. November 2022.

Torres-Freyermuth, A., Mariño-Tapia, I., Coronado, C., Salles, P., Medellín, G., Pedrozo-Acuña, A., Silva, R., Candela, J., Iglesias-Prieto, R., 2012. Wave-induced extreme water levels in the Puerto Morelos fringing reef lagoon. Nat. Hazards Earth Syst. Sci. 12 (12), 3765–3773. https://doi.org/10.5194/nhess-12-3765-2012.

van Dongeren, A., Lowe, R., Pomeroy, A., Trang, D.M., Roelvink, D., Symonds, G., Ranasinghe, R., 2013. Numerical modeling of low-frequency wave dynamics over a fringing coral reef. Coast. Eng. 73, 178–190. https://doi.org/10.1016/j.coastaleng.2012.11.004.

Van Dongeren, A., Reniers, A., Battjes, J., Svendsen, I., 2003. Numerical modeling of infragravity wave response during DELILAH. J. Geophys. Res. Oceans 108 (9), 1–19. https://doi.org/10.1029/2002jc001332.

van Vloten, S.O., Cagigal, L., Rueda, A., Ripoll, N., Méndez, F.J., 2022. HyTCWaves: a Hybrid model for downscaling Tropical Cyclone induced extreme Waves climate. Ocean Model. 178 (April), 102100 https://doi.org/10.1016/j.ocemod.2022.102100.

Wing, O.E.J., Bates, P.D., Sampson, C.C., Smith, A.M., Johnson, K.A., Erickson, T.A., 2017. Validation of a 30 m resolution flood hazard model of the conterminous United States. Water Resour. Res. 53 (9), 7968–7986. https://doi.org/10.1002/2017WR020917.

Zahura, F.T., Goodall, J.L., Sadler, J.M., Shen, Y., Morsy, M.M., Behl, M., 2020. Training machine learning surrogate models from a high-fidelity physics-based model: application for real-time street-scale flood prediction in an urban coastal community. Water Resour. Res. 56 (10) https://doi.org/10.1029/2019WR027038.

Zijlema, M., Stelling, G., Smit, P., 2011. SWASH: an operational public domain code for simulating wave fields and rapidly varied flows in coastal waters. Coast. Eng. 58 (10), 992–1012. https://doi.org/10.1016/j.coastaleng.2011.05.015.